Applied Energy 209 (2018) 392–399

Contents lists available at ScienceDirect

Applied Energy

journal homepage: www.elsevier.com/locate/apenergy

Thermophotovoltaic power conversion using a superadiabatic radiant burner

H. Wu[a], M. Kaviany[b], O.C. Kwon[a,*]

[a] School of Mechanical Engineering, Sungkyunkwan University, Suwon, Gyeonggi-do 10540, Republic of Korea
[b] Department of Mechanical Engineering, University of Michigan, Ann Arbor, MI 48109, USA

HIGHLIGHTS

- A porous superadiabatic radiant burner (SRB) is used for a TPV device.
- The two-layered SiC SRB includes a preheater and radiation corridors.
- Water-cooled GaSb photovoltaic cells are used for the TPV power conversion.
- Emitter efficiencies up to 32% are observed even for fuel-lean condition.
- The SRB-integrated TPV device demonstrates the practical application of the SRB.

ARTICLE INFO

Keywords:
Thermophotovoltaic
Superadiabatic
Porous burners
Heat recirculation
Radiation

ABSTRACT

A new configuration of a 5–10 W thermophotovoltaic (TPV) device integrated with a porous superadiabatic radiant burner (SRB) is suggested and experimentally studied. The silicon carbide (SiC) SRB (emitter) consists of a small-pored upstream section (PM1) and a large-pored downstream section (PM2). PM1 is the section where the incoming fuel-air mixture is preheated internally and PM2 is the section where flame is established. Also, a separate preheater is attached on the SRB to externally recover heat from the exiting flue gas and preheat the inlet air for the burner, and radiation rods are embedded at the interface between the PM1 and PM2 to extract heat from the flame and transfer it to radiating disk surfaces. Radiation from the disk surface is used for the TPV power conversion, reaching gallium antimonide photovoltaic cells (PVCs) with proper quantum efficiencies (up to 80%) through a quartz plate for preventing direct convectional heat transfer from the exhaust gas onto the PVCs. Under optimized conditions, uniform radiation provides adequate TPV performance, particularly indicating reasonable emitter efficiencies (up to 32%) with the enhanced disk temperature even for fuel-lean condition. Thus, the present configuration of the SRB-integrated TPV device can be used in practical applications, avoiding high-level noise without any moving parts.

1. Introduction

In the last two decades, small-scale thermophotovoltaic (TPV) devices which use the direct conversion of thermal energy to electricity via photovoltaic cells (PVCs) have been considered as a strong candidate for a portable power source to replace lithium-ion batteries for portable electronic devices because they have no moving parts and even charge fast and last a long time [1]. Thus, various configurations of gas-fired combustors (emitters) for the small-scale TPV devices have been suggested [2–19].

Power output of a micro TPV power system that consists of a cylindrical silicon carbide (SiC) emitter, a nine-layer dielectric filter and a gallium antimonide (GaSb) PVCs [2] could be enhanced by increasing the backward facing step height of the micro combustor [3], and the effects of the mixture composition and the combustor configuration on the combustion characteristics were also experimentally investigated [4]. A micro cylindrical combustor with rectangular ribs for enhancing heat transfer was numerically investigated [5]. A prototype of the TPV system combined with a thermoelectric (TE) device, using a porous SiC emitter, was built and tested [6]; however, flame is established inside the porous foam, which is not effective for the radiative heat absorbed by PVCs. Also, two TPV prototypes using a non-surface combustion radiant burner and a cascaded radiant burner were tested, showing that porous foam structure demonstrates the best performance [7]. A

* Corresponding author at: School of Mechanical Engineering, Sungkyunkwan University, 2066 Seobu-ro, Jangan-gu, Suwon, Gyeonggi-do 16419, Republic of Korea.
E-mail address: okwon@skku.edu (O.C. Kwon).

http://dx.doi.org/10.1016/j.apenergy.2017.08.168
Received 30 March 2017; Received in revised form 15 August 2017; Accepted 16 August 2017
Available online 31 August 2017
0306-2619/

computational study of a porous medium combustor for improving the combustion stability in a micro-TPV device shows that flame is established at the front of the combustor due to the increased residence time of the fuel-air mixture, resulting in the nonuniform emitter surface temperature and low thermal efficiency [8]. A computational study on the premixed hydrogen (H_2)-air reacting flow inside various non-circular microchannels shows that the combustor with trapezoidal microchannels demonstrates the best performance among the various configurations [9]. Also, studies for improving combustion efficiency by using a heat-recirculation concept have been continuously conducted. For instance, a high temperature recuperative burner was suggested [10]. In this laboratory, novel micro-emitter configurations for micro-TPV devices, adopting the heat-recirculation concept, have been investigated experimentally and computationally [11–15]. A heat-recirculating cylindrical micro-combustor, extracting heat from exhaust gas for preheating the mixture gas, guarantees the stable burning in the small confinement and effective heat transfer into the micro-emitter wall surface for a micro TPV device [11]; however, stainless steel (SS) was used for the test emitter due to the easy fabrication. When the SS emitter was replaced by a SiC emitter under more practical circumstances, the TPV performance has improved [12] and was directly demonstrated using PVCs [13]. The potential of ammonia (NH_3)-H_2 blends as a carbon-free in a micro-TPV device with the heat-recirculating configuration was experimentally evaluated [14], while the potential of integrating a micro-TPV device with a micro-reformer, using NH_3-H_2 blends, has been studied [15]. Additional heat-recirculating combustors which are similar to those in this laboratory but somewhat different in the specific configurations have been suggested by several research groups: a heat-recirculating configuration that involves a swirl combustor and a reverse tube for a miniature TPV device [16], a TPV system which provides both heat and electric power using a combined TPV furnace generator [17], a recuperator for the exhaust gas to preheat fresh air [18] and the utilization of rare earth for selective emitters to enhance the TPV efficiency further [19].

Due to the limited PVC efficiency [15], the aforementioned small-scale TPV devices generally exhibit low overall efficiencies in the range of 0.05–0.95%, though some systems demonstrate relatively higher efficiencies in the range of 2.1–2.3% [7,13,14]. Thus, they seem to be useful for the specific applications such as the military application where the design requirements of fast charging and low-level noise rather than high efficiencies are more important. Nevertheless, enhancing the overall efficiency via improving the combustor efficiency is still meaningful to reduce operating costs. To increase the combustor efficiency the porous ceramic combustors instead of conventional combustors are often adopted due to the concept of their excess enthalpy burning [20]. For the porous ceramic combustors, however, flames are generally established inside the porous medium to maximize the excess enthalpy burning. Thus, if they are adopted for the TPV devices, the radiative heat generated from the flame cannot be effectively absorbed by the PVCs unless there are special radiation corridors between the flame and the PVCs.

A novel porous superadiabatic radiant burner (SRB) with augmented preheating (i.e., internal and external heat-recirculation) and radiation rods (corridors) was recently suggested [21], and its superadiabatic performance has been experimentally demonstrated in this laboratory [22]. The alumina SRB with a square cross-section consists of a fine-pored upstream section to internally preheat the incoming fuel-air mixture and a coarse-pored downstream section to establish flame. A separate preheater is also installed to externally reproduce the heat using the flue gas and warm the inlet air previously for the burner. Finned radiation rods are put at the interface between the two porous media to absorb heat from the flame and the heat is distributed to radiating disk surfaces by the rods. The radiation disk is placed at the downstream end of the radiation rod. Thus, the SRB has the potential of utilization for the TPV power conversion, showing a significant improvement in the performance compared with the conventional porous burners [22]. However, the practical application of the novel SRB has not been demonstrated yet.

Based on these reasons, this experimental study focuses on the design and performance evaluation of a SRB-integrated TPV device as the real application of the SRB. We will first construct the PVC-installed TPV power device applying the SRB referring to the previous research in this laboratory [22]. For this purpose, the detailed dimensions of the SRB have been modified to be integrated with the TPV device as well as to improve the SRB's own performance. As aforementioned, the SRB has a very novel configuration and the unique features [22]. Thus, the present study itself can be considered as the unique study demonstrating the practical application. Then, we will determine the distance between the water-cooled PVCs and the radiation disk surface for avoiding damage to the PVCs due to high operating temperature and maximizing heat irradiation onto the PVCs. Finally, the effects of mixture flow rates and fuel-equivalence ratios on the TPV performance will be observed. Through the experiment, the optimal operating conditions are determined.

2. Experimental methods

A diagram of the experimental apparatus used in this study is given in Fig. 1. It consists of a test TPV device including PVCs and a SRB with two-layer porous media, radiation rods placed in the porous media and a preheater, a fuel-air mixture supply system for the SRB, a water cooling system for the PVCs, a ventilation system, K-type thermocouples for measuring temperature distribution in the SRB and on the PVC surface, a digital camera (Sony A65) for recording the emitter (i.e., the radiation disk) surface and flame images, a spectrometer (Aspec 2048L/Nir256-2.5: 300–2500 nm) for measuring the spectral distribution of the radiating disk surface and a multimeter (Hioki 3803: 0.4000–40.00 V with accuracy of ± 0.6% and 0.4000–10.00 A with accuracy of ± 1.5%) for measuring the electrical output characteristics of the PVCs.

Propane (C_3H_8, purity > 99.9999%) and air (21% O_2/79% nitrogen (N_2) in volume, purity > 99.9%) are supplied respectively to a mixing chamber and to a preheater using commercial mass flow controllers (Area and MKS: 0–200 slm) with accuracy of ± 1.0% of full scale. Calibration for the mass flow controllers was done using a bubble meter and managed by PC-based software (Lab-VIEW) which is able to control fuel-equivalence ratio (ϕ) and the mixture inlet velocity (V) defined as the total volume flow rate of the mixture divided by the cross-sectional area of the SRB, independently. The fuel-equivalence ratio is defined as the fuel-to-air mass ratio of a reacting mixture normalized by the stoichiometric fuel-to-air mass ratio of the corresponding mixture. Thus, $\phi < 1$, $=1$ and > 1 indicate fuel-lean, stoichiometric and fuel-rich conditions, respectively. The preheater using a 10.2 mm (stainless steel, SUS316L) spiral fin tube is located between the downstream end of the porous medium of the SRB and the radiation disks of the radiation rods. It is designed to warm the fresh air using the exhaust gas before the air enters the burner. The preheated air and fuel are mixed in the mixing chamber and are issued from the bottom of a distributor (68 × 68 × 60 mm^3) that is filled with stainless steel beads with an average bead diameter of 1.5 mm for obtaining uniform flow. The distributor is also windowed to detect flashback using quartz. The preheated air-fuel mixture is fed into the porous medium of the SRB with uniform flow.

The SRB consists of a porous medium with fine SiC foam (PM1: 65 ppi (pores per inch), porosity of 0.835, 68 × 68 × 40 mm^3, Ultramet Inc.) upstream and the other porous medium with coarse SiC foam (PM2: 20 ppi, porosity of 0.870, 68 × 68 × 40 mm^3, Ultramet Inc.) downstream. The heat-insulated case with thickness of 5.0 mm (SUS316 L, 78 × 78 × 140 mm^3) surrounds the four sides of porous media. At the exhaust outlet of the burner the preheated air-fuel mixture of near stoichiometric condition is ignited by a torch-igniter. Once the mixture is ignited and a flame is successfully generated, V and ϕ

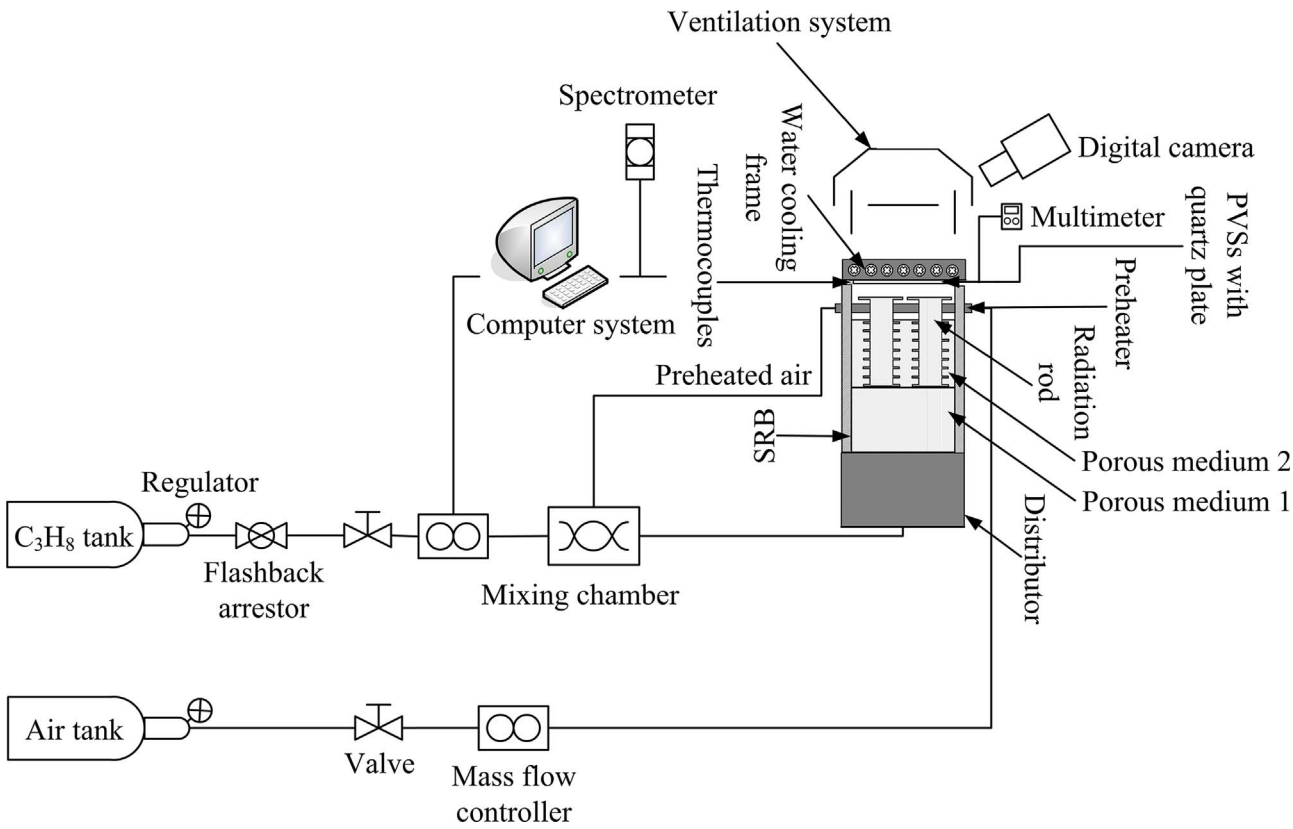

Fig. 1. Schematic of experimental apparatus.

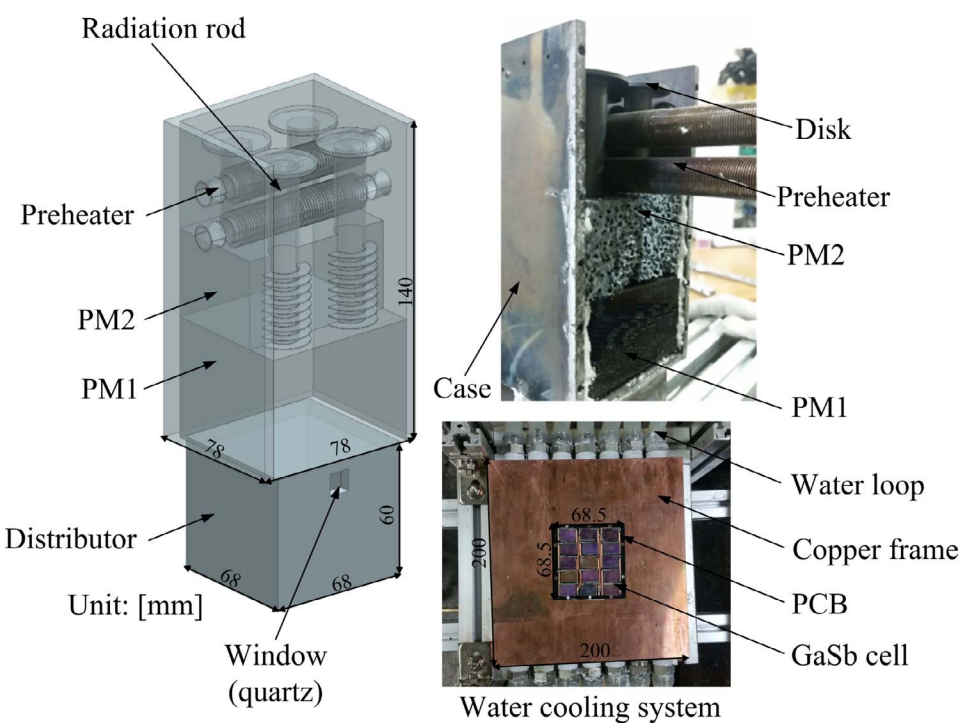

Fig. 2. Assembled and disassembled SRB and water-cooled PVCs.

have been gradually changed to the target values. The flame moves backward and is stabilized in the PM2 through the process of heat transfer between the porous foam and gas. Heat of the flame is absorbed through the fins around the stem of the radiation rods (SiC), transferred through the stem and radiated at the radiation disk towards the PVCs. Thus, the radiation disk surface plays a role as an emitter for the TPV device. Fig. 2 shows the photographs of the assembled and disassembled SRB.

Photovoltaic cells are located at the downstream of the SRB, as shown in Fig. 1. Gallium antimonide cells (JX crystals Inc.) which have the spectral quantum efficiencies of 0.5–0.8 in the 0.7–1.8 μm wavelength, the operating limit temperature of 470 K and a nominal cell efficiency of 10% [23] are used to provide high power density for the present TPV power conversion. Fig. 3 shows the dimensions of a single

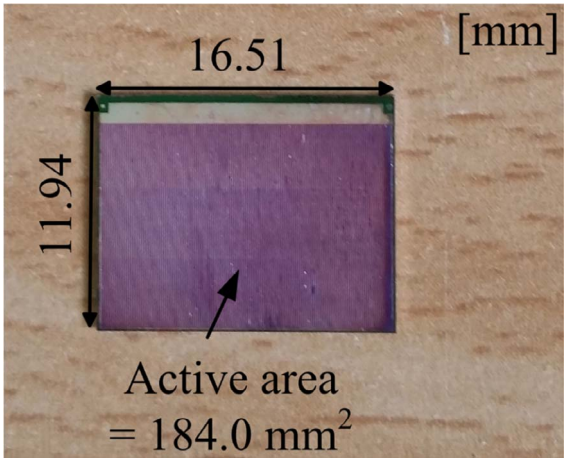

Fig. 3. Dimensions of single GaSb cell.

GaSb cell. Since the increase of the PVC surface temperature hinders the performance of PVCs, a better cooling system of a PVC module has been designed and fabricated, as shown in Fig. 2. The 15 single bus PVCs are attached on a printed circuit board (PCB) with the dimensions of 68.5 × 68.5 × 3.0 mm^3, being connected electrically in series (configurationally three cell arrays in parallel, with each cell array containing series-connected five cells). The PCB is glued onto the bottom wall of the rectangle-shaped water-cooling copper frame (200.0 × 200.0 × 20.0 mm^3) with high thermally conductive paste, having the distance to the radiation disk surface d_g = 11.0–25.0 mm depending on ϕ and V. In the cooling system that is operated by using tap water, water flows through a series of parallel channels (7) drilled into the frame. The copper frame acts as a heat sink for the PVCs, transferring heat to the flowing water. A quartz plate has been placed between the radiation disk surface and the PVCs to prevent the PVCs from the direct exposure by the flue gas.

The temperatures of radiation disk surface and the exhaust gas at the same axial location as the disk surface are measured using K-type thermocouples with a bead diameter of 250 ± 20 μm and accuracy of 5.0%. They are measured for various points at the same axial location and the average values are obtained. The preheated air temperature and the PVC surface temperature are also measured by using K-type thermocouples. Due to the imperfect contact between the solid surface and the thermocouple, however, the radiation disk surface temperature may be underestimated if it is higher than the ambient gas temperature. Thus, it should be noted that the actual disk temperature could be even higher than the reported temperature in Section 3 since it is found to be higher than the exhaust gas temperature at the same axial location. The TPV performance is measured using the spectrometer and the multimeter. Experiments are carried out for C_3H_8-air mixtures of ϕ = 0.60–0.80 and V = 0.227–0.351 m/s at a temperature (298 ± 3 K) and atmospheric pressure (normal temperature and pressure, NTP). Final results are obtained by averaging measurements of 4–5 tests at each condition. Experimental uncertainties (95% confidence) for V and T are estimated to be less than 5%.

3. Results and discussion

3.1. Configuration and dimensions of SRB-integrated TPV device

Based on the previous study of the SRB [22], the final configuration and dimensions of the TPV device have been determined to have the two-layered SRB including a preheater and radiation rods as briefly described in Section 2 (Fig. 2).

The basic geometry of the SRB is a square cylindrical configuration because the simple structured is to equip the uniformly radiating burner and to utilize the external heat-recirculation concept of recovering heat from exhaust gas with the preheater. Combustion in the PM2 releases heat, and then it is absorbed and transferred through the fins around the stem of the radiation rods and the stem, respectively. It is finally radiated at the radiation disk surface. The cross-sectional area of the PM1 and PM2 and the number of radiation rods (4) and PVCs (15 single bus cells) have been established on the base of the limited capability of the present mass flow controllers. The dimensions of the stem, fin and disk of the radiation rod and the preheater and the pore size and thickness of the PM1 and PM2 have been determined based on the earlier studies of the SRB [21,22] and the feasibility of fabrication. For decreasing the thermal resistance of the radiation rod, diameter of the radiation rod has been increased compared with the previous alumina SRB developed in this laboratory [22] so that the performance (i.e., the radiation disk surface temperature and the radiation efficiency) of the system can be improved.

The present GaSb cells have a band gap of 0.726 eV and the active area of 184.0 mm^2. It implies that the spectra of the SiC broadband emitter should not contain a significant portion of photons with the wavelength > 1.8 μm. In theory, this requires an emitter which can run around 1700 K [23] because we do not use a dielectric filter between the emitter and PVCs in this study. Table 1 shows the specifications of the major components of the SRB-integrated TPV device, which includes the detailed dimensions and materials.

3.2. Performance of emitter (radiation disk surface)

In order to enhance the internal heat recirculation and maximize radiation from the radiation disk, both the porous foam and the radiation rods are made of SiC. The radiating disk surface temperature and the flue gas temperature at the same axial location have been

Table 1
Specifications of major components of SRB-integrated TPV device.

Components	Parameters	Values
PM1	Materials	Silicon carbide (SiC)
	Width (height)	68.0 mm
	Length	40.0 mm
	Porosity	0.835
	Pore size	65 ppi
	Thermal conductivity	1.14 W/m-K
PM2	Materials	SiC
	Width (height)	68.0 mm
	Length	40.0 mm
	Porosity	0.870
	Pore size	20 ppi
	Thermal conductivity	1.34 W/m-K
Radiation rods	Materials	SiC
	Stem diameter	14.0 mm
	Fin diameter	24.0 mm
	Fin thickness	1.5 mm
	Fin pitch	333 m^{-1}
	Disk diameter	32.0 mm
	Disk thickness	2.0 mm
	Length	90.0 mm
Preheater (fin tube)	Materials	Stainless steel (SUS316L)
	Inner diameter	10.2 mm
	Fin diameter	16.0 mm
	Fin thickness	1.0 mm
	Fin pitch	666 m^{-1}
	Tube thickness	0.5 mm
	Length	70.0 mm
Photovoltaic cells	Materials	Gallium antimonide (GaSb)
	Length	16.51 mm
	Width	11.94 mm
	Active area	184.0 mm^2
	Thickness	0.65 mm
	Grid width	0.016 mm
	Grid spacing	0.102 mm

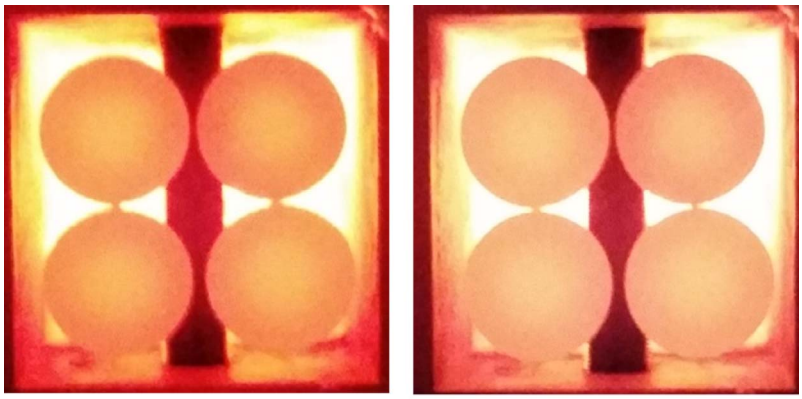

Fig. 4. Images of radiating PM2 and radiation disks for premixed C_3H_8/air flames of ϕ = 0.70 (a) and 0.80 (b) in SRB at NTP: fuel flow rate of 2400 sccm.

measured, from which the disk surface temperature higher than the exhaust gas is expected and the best operating condition of the SRB in the consideration of safe operation within the present test conditions is determined.

Due to the limited melting point of SiC foam experiments have been conducted at the fuel-equivalence ratio up to 0.8. Also, the present GaSb cells ideally require an emitter operating around 1700 K as discussed in Section 3.1 and thus only the condition of $\phi \geq 0.7$ has been considered to maintain at least 1250 K for all the present fuel flow rates, though the SRB could operate even at ϕ = 0.24. Fig. 4a and b shows the images of the radiating PM2 and radiation disks for the premixed C_3H_8/air flames of ϕ = 0.7 and 0.8, respectively. These images clearly exhibit intensified radiation due to the enhanced burning for enhanced ϕ under fuel-lean condition. This tendency is confirmed from the temperature measurements on the radiation disk surface. Figs. 5 and 6 show the measured disk surface and flue gas temperature at the same axial location as a function of fuel flow rates for the premixed C_3H_8/air flames of ϕ = 0.7 and 0.8, respectively. As expected, the disk surface temperature is higher for ϕ = 0.8. For both ϕs, however, the disk and flue gas temperatures rise as the gas mixture burns with increasing fuel flow rates in the PM2. Since the superadiabatic effects of the SRB occurs due to both the internal and external heat recirculation, the radiation disk surface temperature is higher than the flue gas temperature under all the test conditions. The temperature difference between the disk surface and local exhaust gas is 27–43 K and 14–25 K (but actually larger gaps expected as discussed in Section 2) for ϕ = 0.70 and 0.80, respectively. These results exhibit that the superadiabatic effect is stronger at the fuel-leaner condition, indicating that the flame temperature increases but the heat losses to the surroundings through the

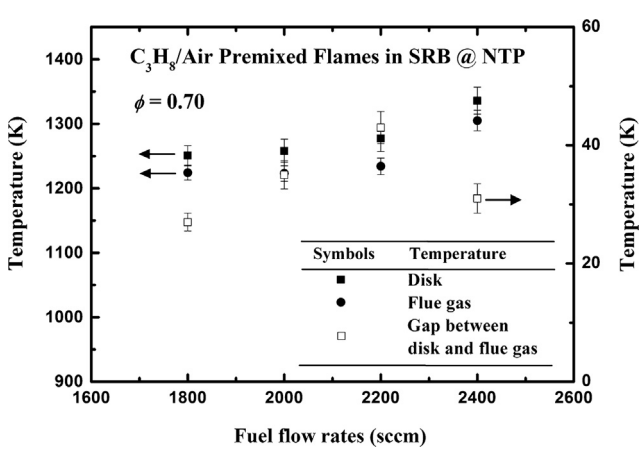

Fig. 5. Disk and flue gas temperature in terms of fuel flow rates for premixed C_3H_8/air flames of ϕ = 0.70 in SRB at NTP.

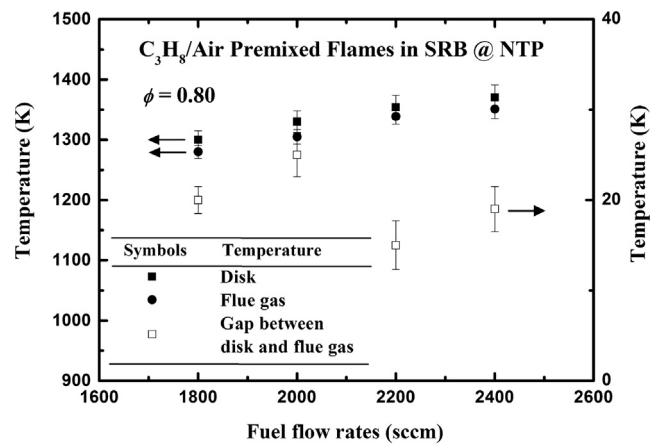

Fig. 6. Disk and flue gas temperature in terms of fuel flow rates for premixed C_3H_8/air flames of ϕ = 0.80 in SRB at NTP.

side walls of the PM2 is relatively reduced with increasing ϕ. Based on these observations, i.e., the higher disk surface temperature for ϕ = 0.80 but the larger temperature difference between the disk surface and local exhaust gas for ϕ = 0.70 that may result in higher radiation efficiency, both the fuel-equivalence ratios have been considered to determine the optimized distance between the radiation disk surface and the PVC surface (d_g), which will be discussed in Section 3.3.

3.3. Effects of distance between emitter and PVC surfaces

In order to accommodate the high efficiency of the SRB-integrated TPV device, further thermal management steps such as the cooling of PVCs must be implemented. As described in Section 2, a cooling system which is operated by supplying tap water in the copper frame as a heat sink is utilized in the present study. The temperature on the PVC surface influences the output power and saturation current of the SRB-integrated TPV device: the performance will substantially degrade if it is higher than the operating limit temperature (≈470 K) for the GaSb cells [23]. Figs. 7 and 8 show the maximum temperature on the PVC surface with various d_g as a function of time (after flame is stabilized in the SRB) for the premixed C_3H_8/air flames of the fuel flow rate of 2400 sccm and ϕ = 0.70 and 0.80, respectively. As expected, the maximum temperature of the PVC surface increases with increasing ϕ. For ϕ = 0.70 it is 482, 454 and 435 K respectively with d_g = 11, 15 and 21 mm, while for ϕ = 0.80 508, 480, 448 and 430 K respectively with d_g = 11, 15, 21 and 25 mm. A longer distance leads to less emissive power, while a shorter distance increases the risk of damage to the PVC. Of course, a smaller distance between the radiation disk and PVC surfaces can be achieved by improving the cooling efficiency with the

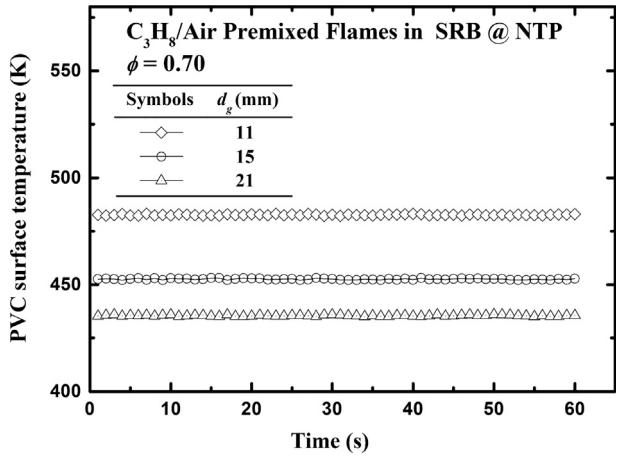

Fig. 7. Maximum temperature on PVC surface with various d_g as function of time for premixed C_3H_8/air flames of ϕ = 0.70 and fuel flow rate of 2400 sccm in SRB-integrated TPV device at NTP.

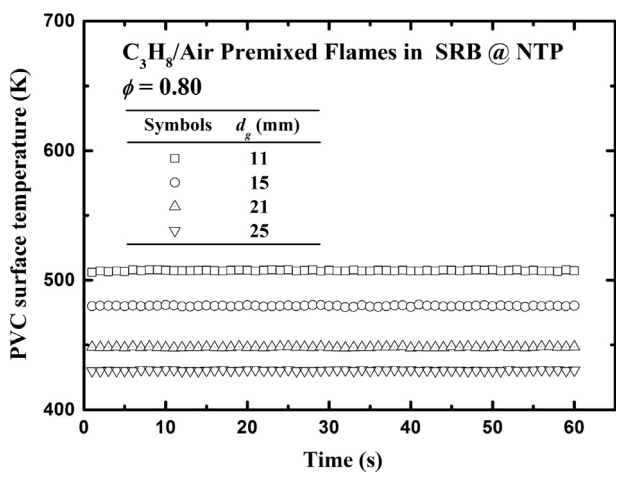

Fig. 8. Maximum temperature on PVC surface with various d_g as function of time for premixed C_3H_8/air flames of ϕ = 0.80 and fuel flow rate of 2400 sccm in SRB-integrated TPV device at NTP.

utilization of a compressor; however, extra power is required to drive the compressor. Considering the limited electric output power and overall system efficiency of the present SRB-integrated TPV device, which will be discussed in Section 3.4, the compressor has not been adopted, directly using the tap water. In the present study, the flow rate of water is 21.2 L/min, which is the maximum flow rate of the tap water in this laboratory. Thus, the results in Figs. 7 and 8 and the operating limit temperature for the GaSb cells indicate that d_g = 21 mm is found to be the proper distance between the emitter and PVC surfaces in the present SRB-integrated TPV device.

3.4. Performance of SRB-integrated TPV device

The spectral distribution of the emitter (i.e., the radiating disk surface) has been measured to understand the spectral characteristics of heat irradiation onto the GaSb cells. Based on the results in Section 3.3, the measurements have been conducted for d_g = 21 mm.

Figs. 9 and 10 show the measured emissive power density onto the GaSb cells as a function of wavelengths for the premixed C_3H_8/air flames of the fuel flow rate of 2400 sccm and ϕ = 0.70 and 0.80 in the SRB-integrated TPV device, respectively. In the 700–1800 nm wavelength where the present GaSb cells can properly generate power [23], higher emissive power density is generally found for ϕ = 0.80 because of the enhanced emitter surface temperature due to the intensified

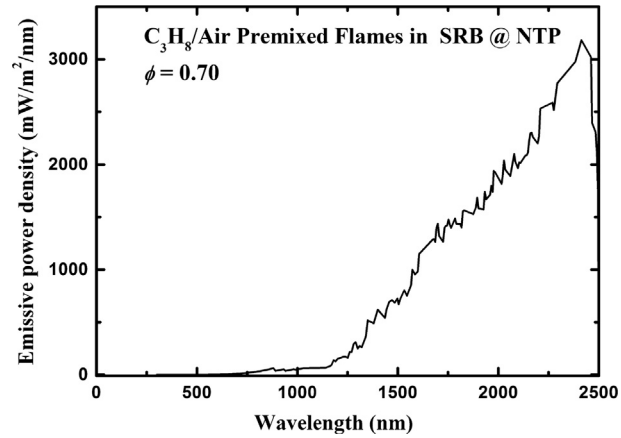

Fig. 9. Emissive power density on radiative disk surface for premixed C_3H_8/air flame of ϕ = 0.70 and fuel flow rate of 2400 sccm in SRB-integrated TPV at NTP (d_g = 21 mm).

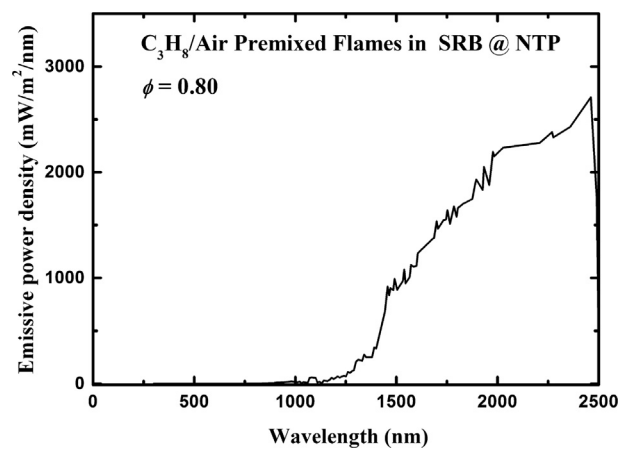

Fig. 10. Emissive power density on radiative disk surface for premixed C_3H_8/air flame of ϕ = 0.80 and fuel flow rate of 2400 sccm in SRB-integrated TPV at NTP (d_g = 21 mm).

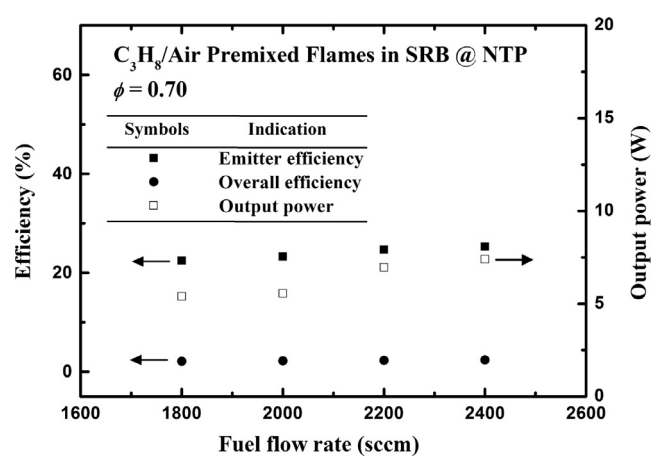

Fig. 11. Emitter efficiency, overall efficiency and output power of SRB-integrated TPV device for premixed C_3H_8/air flames of ϕ = 0.70 and various fuel flow rates at NTP (d_g = 21 mm).

combustion of the SRB.

As the overall performance of the SRB-integrated TPV device with d_g = 21 mm, Figs. 11 and 12 show emitter efficiency, overall efficiency and output power as a function of fuel flow rates for the premixed C_3H_8/air flames of ϕ = 0.70 and 0.80 at NTP, respectively. The emitter efficiency (Eq. (1)) of the SRB-integrated TPV device can be defined as the ratio of the radiant power on the radiation disk surface to the total

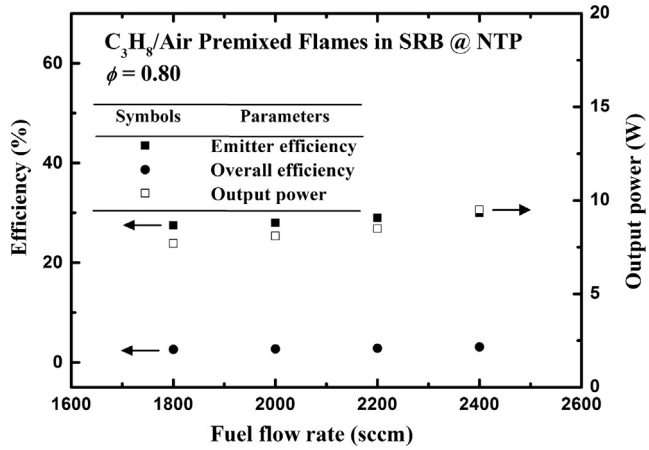

Fig. 12. Emitter efficiency, overall efficiency and output power of SRB-integrated TPV device for premixed C_3H_8/air flames of ϕ = 0.80 and various fuel flow rates at NTP (d_g = 21 mm).

Table 2
Optimized configuration and operating conditions and performance of SRB-integrated TPV device.

Configuration, operation and performance parameters	Values
Materials	Emitter: SiC PVCs: GaSb
Distance between emitter surface and GaSb cell surface (d_g)	21 mm
Fuel flow rate	2400 sccm
Equivalence ratio (ϕ)	0.8
Emitter efficiency	32.1%
Electrical output power	9.5 W
Overall system efficiency	3.1%

chemical heat input rate, while the overall efficiency (Eq. (2)) as the ratio of the electrical power output to the total chemical energy input rate:

$$\eta_{emitter} = \frac{P_{rad(net)}}{H_{fuel}\dot{m}} = \frac{\int_0^\infty W_s(\lambda,T)\varepsilon_{SiC}S_E d\lambda}{H_{fuel}\dot{m}} = \frac{\sigma T^4 \varepsilon_{SiC} S_E}{H_{fuel}\dot{m}} \quad (1)$$

$$\eta_{overall} = \frac{P_{electrical}}{H_{fuel}\dot{m}} \quad (2)$$

where σ, T, ε_{SiC}, S_E, H_{fuel} and $\dot{m}$ are the Stephan-Boltzmann constant, the emitter temperature, the SiC emissivity, the effective area of the radiation disk, the lower heating value of the fuel and the mass flow rate of fuel, respectively.

For ϕ = 0.70 both the overall efficiency and output power increase with increasing fuel flow rates. The maximum output power (7.4 W), emitter efficiency (27.4%) and overall efficiency (2.4%) are found at the fuel flow rate of 2400 sccm where the maximum emitter temperature is observed. For ϕ = 0.80 the maximum output power (9.5 W), emitter efficiency (32.1%) and overall efficiency (3.1%) are again observed at the fuel flow rate of 2400 sccm. Thus, for the present configuration and materials of the SRB-integrated TPV device and test conditions the overall efficiency ranges from 2.4% to 3.1%, which is a similar level to that of conventional TPV devices. This seems to be caused by the fuel-lean combustion in the SRB since the SRB-integrated TPV device could not operate at the stoichiometric condition due to the limited melting points of the foam and radiation corridors. It is also expected that heat is lost through the side walls of the SRB to the ambient. The optimized configuration and operating conditions and the performance of the present SRB-integrated TPV device are summarized in Table 2.

So far, we have considered the SRB-integrated TPV device as the application of the SRB that has a very novel configuration and the unique features and was developed in the earlier study [22]. The results clearly demonstrate the potential of the SRB in real applications, i.e., the TPV application. Although the present SRB-integrated TPV device can be considered as a stand-alone TPV system, its further application seems possible. Since the heat-recirculation concept is adopted in the present device, a substantial amount of heat is already recovered, but still a considerable amount of heat is lost through the side walls of the PM2 and the exhaust gas. Also, considering that perfect thermal insulation is not possible, it will be reasonable to utilize the lost (through the side walls) and exhausted (after the preheater) heat for heating in addition to the power generation of the SRB-integrated TPV device. In this laboratory, a small and quiet portable TPV power generation system adopting photonic crystal structure is under development for military applications as introduced in Section 1 [24]. For the system a cylindrical heat-recirculating combustor is currently used, but the present SRB-integrated TPV device will be also considered for both the electrical power from the emitter (i.e., the radiation disks) and the heating from the exhaust gas.

4. Conclusions

In the present investigation the potential of the concept of a thermophotovoltaic (TPV) device integrated with a superadiabatic radiant burner (SRB, i.e., a radiant porous burner with augmented preheating) was experimentally evaluated. The SRB-integrated TPV device was designed and fabricated, and the radiant surface (emitter) temperature distribution, the spectral characteristics on the emitter, the emitter efficiency, the overall efficiency and output power were measured. The major conclusions of this study are as follows:

1. A new configuration of the 5–10 W TPV device with water-cooled GaSb photovoltaic cells that is integrated with the porous SiC SRB with a square cross-section, a small-pored upstream section, a large-pored downstream section, a preheater and SiC radiation corridors has been successfully fabricated.
2. The superadiabatic effects of the SiC SRB have been confirmed and enhanced compared with the previous alumina SRB, due to the new materials and the decreased thermal resistance of the radiation corridor.
3. Under optimized design and operation conditions, uniform radiation provides adequate TPV performance, particularly indicating reasonable efficiencies with the enhanced emitter temperature even for fuel-lean condition. Thus, the proposed configuration of the SRB-integrated TPV device in this study can be used in practical applications, avoiding high-level noise with no moving parts.

Acknowledgement

This research was supported by Basic Science Research Program through the National Research Foundation of Korea (NRF) funded by the Ministry of Education (No. 2013R1A1A2006403) and by Advanced Research Center Program (NRF-2013R1A5A1073861) through the NRF grant funded by the Korea Government (MSIP) contracted through Advanced Space Propulsion Research Center at Seoul National University.

References

[1] Fernandez-Pello C. Micropower generation using combustion: issues and approaches. Proc Combust Inst 2002;29:883–99.
[2] Yang WM, Chou SK, Shu C, Xue H, Li ZW. Development of a prototype micro-thermophotovoltaic power generator. J Phys D: Appl Phys 2004;37:1017–20.
[3] Yang WM, Chou SK, Shu C, Li ZW, Xue H. Experimental study of micro-thermophotovoltaic systems with different combustor configurations. Energy Convers Manage 2007;48:1238–44.
[4] Pan JF, Huang J, Li DT, Yang WM, Tang WX, Xue H. Effects of major parameters on

micro-combustion for thermophotovoltaic energy conversion. Appl Therm Eng 2007;27:1089–95.
[5] Zuo W. E J, Liu H, Peng Q, Zhao X, Zhang Z. Numerical investigations on an improved micro-cylindrical combustor with rectangular rib for enhancing heat transfer. Appl Energy 2016;184:77–87.
[6] Qiu K, Hayden ACS. Development of a novel cascading TPV and TE power generation system. Appl Energy 2012;91:304–8.
[7] Qiu K, Hayden ACS. Thermophotovoltaic power generation systems using natural gas-fired radiant burners. Sol Energy Mater Sol Cells 2007;91:588–96.
[8] Pan JF, Wu D, Liu YX, Zhang HF, Tang AK, Xue H. Hydrogen/oxygen premixed combustion characteristics in micro porous media combustor. Appl Energy 2015;160:802–7.
[9] Akhtar S, Kurnia JC, Shamim T. A three-dimensional computational model of H_2-air premixed combustion in non-circular micro-channels for a thermo-photovoltaic (TPV) application. Appl Energy 2015;152:47–57.
[10] Mattarolo G. High temperature recuperative burner. In: 1st conference for thermophoto-voltaics: science to business, January 27, Berlin, Germany; 2005.
[11] Lee KH, Kwon OC. Studies on a heat-recirculating micro-emitter for a micro thermophotovoltaic system. Combust Flame 2008;153:161–72.
[12] Park JH, So JS, Moon HJ, Kwon OC. Measured and predicted performance of a micro-thermophotovoltaic device with a heat-recirculating micro-emitter. Int J Heat Mass Trans 2011;54:1046–54.
[13] Park JH, Lee SI, Wu H, Kwon OC. Thermophotovoltaic power conversion from a heat-recirculating micro-emitter. Int J Heat Mass Trans 2012;55:4878–85.
[14] Lee SI, Um DH, Kwon OC. Performance of a micro-thermophotovoltaic power system using an ammonia-hydrogen blend-fueled micro-emitter. Int J Hydrogen Energy 2013;38:9330–42.
[15] Um DH, Kim TY, Kwon OC. Power and hydrogen production from ammonia in a micro-thermophotovoltaic device integrated with a micro-reformer. Energy 2014;73:531–42.
[16] Li Y-H, Li H-Y, Dunn-Rankin D, Chao Y-C. Enhancing thermal, electrical efficiencies of a miniature combustion-driven thermophotovoltaic system. Prog Photovolt: Res Appl 2009;17:502–12.
[17] Fraas LM, Avery JE, Huang HX. Thermophotovoltaic furnace-generator for the home using low bandgap GaSb cells. Semicond Sci Technol 2003;18:247–53.
[18] Ferrari C, Melino F, Bosi M. The critical role of emitter size in thermo-photovoltaic generators. Sol Energ Mater Sol Cells 2013;113:20–5.
[19] Ferrari C, Melino F, Pinelli M, Spina PR. Thermophotovoltaic energy conversion: Analytical aspects, prototypes and experiences. Appl Energy 2014;113:1717–30.
[20] Hardesty DR, Weinberg FJ. Burners producing large excess enthalpies. Combust Sci Technol 1974;8:201–14.
[21] Vandadi V, Park C, Kaviany M. Superadiabatic radiant porous burner with preheater and radiation corridors. Int J Heat Mass Trans 2013;64:680–8.
[22] Wu H, Kim YJ, Vandadi V, Park C, Kaviany M, Kwon OC. Experiment on superadiabatic radiant burner with augmented preheating. Appl Energy 2015;156:390–7.
[23] JX Crystals Inc. Specifications of GaSb cells. Issaquah (WA): JX Crystals Inc; 2008.
[24] Kim TY, Kim HK, Ku JW, Kwon OC. A heat-recirculating combustor with multiple injectors for thermophotovoltaic power conversion. Appl Energy 2017;193:174–81.